Talanta 84 (2011) 538–546

Contents lists available at ScienceDirect

Talanta

journal homepage: www.elsevier.com/locate/talanta

Carbon nanotube-based symbiotic coaxial nanocables with nanosilica and nanogold particles as labels for electrochemical immunoassay of carcinoembryonic antigen in biological fluids

Qunfang Li [a], Dianping Tang [a,*], Juan Tang [a], Biling Su [a], Jianxin Huang [b], Guonan Chen [a,*]

[a] Ministry of Education Key Laboratory of Analysis and Detection for Food Safety, Fujian Provincial Key Laboratory of Analysis and Detection Technology for Food Safety, Department of Chemistry, Fuzhou University, Fuzhou 350108, PR China
[b] Clinical Laboratory and Medical Diagnostics Laboratory, Fujian Provincial Hospital, Fuzhou 350001, PR China

ARTICLE INFO

Article history:
Received 3 November 2010
Received in revised form 16 January 2011
Accepted 25 January 2011
Available online 1 February 2011

Keywords:
Carbon nanotube
Electrochemical immunosensor
Symbiotic coaxial nanocables
Nanogold particles
Carcinoembryonic antigen
Silica nanoparticles

ABSTRACT

A feasible and practicable amperometric immunoassay strategy for sensitive screening of carcinoembryonic antigen (CEA) in human serum was developed using carbon nanotube (CNT)-based symbiotic coaxial nanocables as labels. To construct such a nanocable, a thin layer of silica nanoparticles was coated on the CNT surface by sonication and sol–gel methods, and then colloidal gold nanoparticles were assembled on the amino-functionalized SiO_2/CNTs, which were used for the label of horseradish peroxidase-anti-CEA conjugates (HRP-*anti*-CEA-Au/SiO_2/CNT). In the presence of analyte CEA, the sandwich-type immunocomplex was formed on an anti-CEA/Au/thionine/Nafion-modified glassy carbon electrode by using HRP-*anti*-CEA-Au/SiO_2/CNTs as detection antibodies. To embody the advantages of the protocol, the analytical properties of variously modified electrodes were compared in detail on the basis of different nanolabels. Under optimal conditions, the cathodic peak currents of the electrochemical immunosensor were proportional to the logarithm of CEA concentration over the range from 0.01 to 12 ng mL^{-1} in pH 5.5 HAc-NaAc containing 5 mM H_2O_2. At a signal-to-noise ratio of 3, the detection limit (LOD) is 5 pg mL^{-1} CEA. Intra- and inter-assay coefficients of variation were below 9.5%. Meanwhile, the selectivity and stability of the immunosensor were acceptable. In addition, the technique was evaluated by spiking CEA standards in pH 7.4 PBS and with 35 clinical serum specimens, receiving excellent accordance with results from commercially available electrochemiluminescent enzyme-linked immunoassay.

1. Introduction

Electrochemical immunosensors and immunoassays, based on the specificity of antigen–antibody interactions with electrochemical transducers, have become fascinating subjects for clinical diagnosis, food analysis, environmental monitoring, and other fields during past decades [1]. Among them, a sensitive and simple method for detection of disease-related proteins has attracted increasing interest [2,3]. It is well known that carcinoembryonic antigen (CEA) is a protein found in many types of cells with tumors and the developing fetus. The normal range is below 2.5 ng mL^{-1} in an adult non-smoker and 5.0 ng mL^{-1} in a smoker [4]. Benign conditions and diseases do not usually cause a CEA increase over 10 ng mL^{-1}. However, the most common cancers that elevate CEA are in most human colorectal, gastric and pancreatic carcinomas as well as several other carcinomas. Level over 20 ng mL^{-1} before therapy is associated with cancer, which has already metastasized (spread) [5]. Numerous electrochemical immunosensors and immunoassays for CEA determination combined with potentiometric, amperometric, conductometric and impedance transducers have been reported [6–9]. Despite many advances in the field, it is still a challenge to explore and exploit new schemes and strategies for improvement of the sensitivity and simplicity of electrochemical immunosensors.

In the electrochemical immunoassays, sandwich-type and competitive-type binding protocols are the most popular modes for the antigen/antibody detection [2]. Owing to the use of two matched antibodies in the sandwich assay, i.e. a sandwich with the antigen and a conjugate with an antibody (which combines with another epitope of the antigen and the label), it has the advantages of high specificity and high sensitivity [10]. Usually, the measurable signal is difficultly achieved from a direct immunoreaction, thus an appropriate label is indispensable [11]. The classical example is based on enzyme-labeled secondary antibody. However, the association constant for small analyte–antibody complexes may be as high as 10^{10}–10^{12} M^{-1}, and creating a further increase is almost impossible [12]. There is because of sterical reasons usually a ratio

* Corresponding authors. Tel.: +86 591 2286 6125; fax: +86 591 2286 6135.
E-mail addresses: dianping.tang@fzu.edu.cn, dianping.tang@hotmail.com (D. Tang), gnchen@fzu.edu.cn (G. Chen).

0039-9140/$ – see front matter © 2011 Elsevier B.V. All rights reserved.
doi:10.1016/j.talanta.2011.01.063

of 1:1 for enzyme and secondary antibody used in the traditional enzyme immunoassay. We might suspect that the sensitivity might be enhanced if more enzyme molecules are labeled on one antibody. It is impossible due to the limitation of the binding sites, but.

The emerging research field of nanoscale-enabled technology provides excitingly new possibility for advanced development of newly labeled methods and techniques in the electrochemical immunoassays [13]. Variously nanoscales-based labeling probes have employed for development of electrochemical immunoassays, e.g. nanogold-coated mesoporous nanosilica particles [14], graphene nanosheets [15], Pt nanoparticles [16], biotin–streptavidin [17], dumbbell-like Au–Fe_3O_4 nanoparticles [18], and Pt hollow nanospheres [19]. Recently, we tried to fabricate several nanolabels for the electrochemical immunoassays, such as magnetic nanogold microspheres [20], nanogold hollow microspheres [21], enzyme-nanosilica-doped carbon nanotubes [22], gold nanoparticle-decorated poly(amidoamine) dendrimer [23], irregular-shaped gold nanoparticles [24], and double-codified gold nanoparticles [25]. Experimental results indicated that the sensitivity and dynamic range of the electrochemical immunosensor could be improved to some extent using the nanolabels. Further investigations are to employ the nanowires, nanotubes and nanofibers as labels due to their unique structures and properties [26].

Carbon nanotubes (CNTs, also known as buckytubes) are considered as one of the most fascinating candidates due to their high tensile strength coupled with high surface area, high electronic conductivity, and thermal conductivity [27]. Since it is difficult for CNTs to disperse homogeneously in solution due to the formation of big bundles held strongly together, it is necessary to functionalize the CNTs [28]. Inorganic nanoparticles/CNT hybrid materials, possessing the properties of each component with a synergistic effect, have charmed more interest [29]. Nanosized silica has been proved to be an ideal protein host due to its excellent surface properties and inherent stability [30]. Lin and Shen demonstrated that single-walled carbon nanotubes could be coated by a thin layer of silica through the reaction between chlorosilane and acid-treated CNTs [31]. Peng et al. reported a new method of noncovalently functionalizing CNTs with an organic–inorganic hybrid silica for constructing superhydrophobic conductive coatings [32]. However, the biomolecules were usually immobilized on the CNT/SiO_2 surface *via* the covalent binding [33–35]. One of the problems commonly associated with covalent binding is the decrease of protein bioactivity when the biomolecules are exposed to reactive groups and harsh reaction conditions. On the contrary, gold nanoparticles (Aus) could provide a suitable microenvironment similar to the native environment of bioconjugates [36]. Wang group introduced a simple method of synthesizing gold/platinum hybrid nanoparticles supported on CNT/SiO_2 coaxial nanocables [37]. It was found that the as-prepared Au/SiO_2/CNTs displayed a high electrocatalytic activity for oxygen reduction.

Herein, we tried to construct a new sandwich-type electrochemical immunoassay method for detection of CEA (as a model biomarker) by using CNT-based symbiotic coaxial nanocables as labels. Gold nanoparticles-coating coaxial nanocables could be easily synthesized on the SiO_2/CNTs by using amino-functionalized silica. The attached gold nanoparticles on the nanocables were utilized for the label of HRP-anti-CEA antibodies (bionanocables). The content of CEA was assayed on an anti-CEA/Au/thionine/Nafion-modified glassy carbon electrode using the as-prepared bionanocables as traces and H_2O_2 as enzyme substrates. The aim of this study is to explore a nanocable-based labeling method for development of sensitized sandwich electrochemical immunoassay.

2. Experimental

2.1. Chemicals and materials

Monoclonal anti-CEA antibody produced in mouse (anti-CEA, clone C6G9), HRP-labeled monoclonal mouse *anti*-CEA antibody (HRP-*anti*-CEA), and CEA standards (0, 5, 10, 20, 40 and 80 ng mL^{-1}) were purchased from Biocell Biotechnol. Co., Ltd. (Zhengzhou, China). Thionine acetate salt (TH, Dye content ≥85%), Nafion® 117 solution (NF, purum, 5% in mixture of lower aliphatic alcohols and water), Tetramethoxysilane (TEOS, 98%), (3-aminopropyl)triethoxysilan (APTES, 97%), polyvinylpyrrolidone (PVP, average mol wt 10,000), bovine serum albumin (BSA, lyophilized powder, ~66 kDa), and sodium citrate tribasic hydrate were obtained from Sigma–Aldrich. $HAuCl_4{\cdot}4H_2O$ was purchased from Sinopharm Chem. Re. Co., Ltd. (Shanghai, China). Single-walled carbon nanotubes (CNTs, CVD method, purity ≥98%, diameter 5–10 nm, and length 1–2 μm) were supplied by Shenzhen Nanoport Co., Ltd. (Shenzhen, China). 16-nm gold colloids were synthesized according to our previous protocol [38]. Deionized and distilled water was used throughout the study. 0.1 M acetic acid-buffered saline (ABS) with various pHs were prepared by mixing the stock solutions of 0.1 M HAc and 0.1 M NaAc, and 0.1 M KCl was added as the supporting electrolyte. Phosphate-buffered saline (PBS, 0.1 M) of various pHs were prepared by mixing of the stock solutions of 0.1 M Na_2HPO_4 and 0.1 M NaH_2PO_4. All other chemicals used were of analytical reagent grade and were used without further purification. Clinical serum samples were gifted from Fujian Provincial Hospital, China.

2.2. Apparatus

Electrochemical measurements were carried out with a CHI 620D Electrochemical Workstation (Shanghai CH Instruments Inc., China). Electrochemical impedance spectroscopy (EIS) was performed on a CHI 604D Electrochemical Workstation (Shanghai CH Instruments Inc., China). Carbon nanotube (CNT)-based symbiotic coaxial nanocables were characterized by using Tecnai G2 F20 transmission electron microscopy (TEM, USA). Fourier-transform infrared spectroscopic (FT-IR) characteristics of Au/SiO_2/CNTs and Au/SiO_2/CNTs with the immobilized HRP-*anti*-CEA were characterized by FT-IR system (Perkin-Elmer Spectrum 2000, USA). X-ray photoelectron spectroscopy (XPS) measurements were carried out using a VG Scientific ESCALAB 250 spectrometer with Al Kα X-ray (1486.6 eV). Clinical serum samples were assayed using Elecsys 2010 Electrochemiluminescent Automatic Analyzer (Roche, Switzerland).

2.3. Synthesis and bioconjugation of Au/SiO_2/CNT nanocables

Au/SiO_2/CNT nanocables were synthesized according to the literature [37] with a little modification as follows: (i) the shorted CNTs were prepared by continuously sonicating the CNTs in a mixture solution containing H_2SO_4 and HNO_3 (3:1, v/v) for 4 h; (ii) 45 mL PVP aqueous solution (0.5%, w/w) containing 9 mg CNTs was sonicated for 2 h, and the mixture was centrifuged and diluted into 10 mL ethanol solution ($C_{[CNT]} \approx 90$ mg mL^{-1}); (iii) 5 mL ammonia (25–28%, w/w) and 300 μL TEOS (98%, w/w) were added into the PVP/CNT solution in turn, and continuously sonicated for 12 h at room temperature (RT); (iv) 200 μL APTES (97%) and 200 μL ammonia (25–28%, w/w) were injected in the colloidal SiO_2/PVP/CNTs in order, and stirred at 800 rpm for 12 h at RT; and (v) 100 mL gold colloids ($C_{[Au]} = 24$ mM) was added into the APTES/SiO_2/PVP/CNTs precipitation obtained by centrifugation, and slightly stirred at 150 rpm for 6 h. Finally, the purified gold nanoparticles supported symbiotic coaxial nanoca-

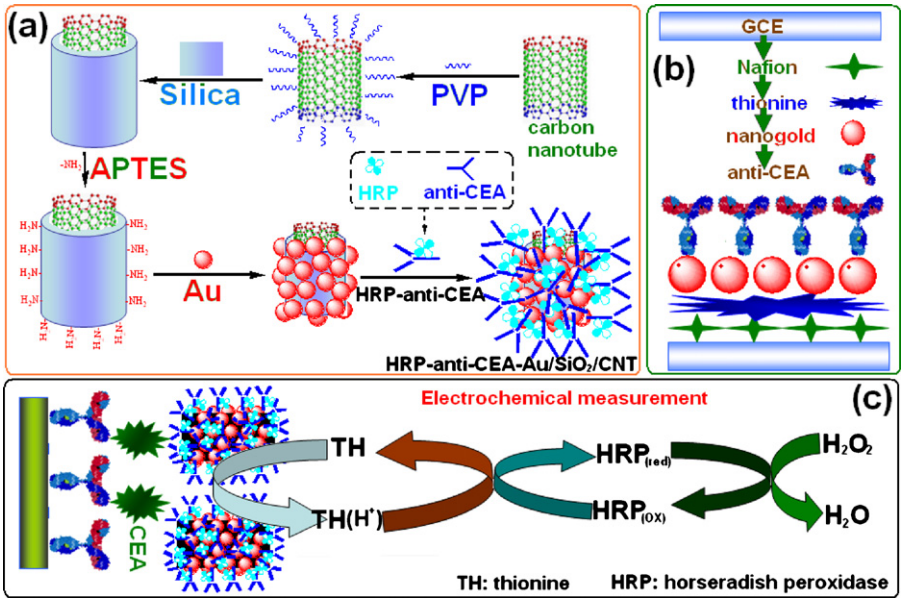

Scheme 1. (a) Fabrication process of HRP-*anti*-CEA-Au/SiO_2/CNT symbiotic coaxial bionanocables, (b) structural representation of the electrochemical immunosensor, and (c) the schematic illustration of the sandwich-type immunocomplex on the electrode surface and the redox process of the electrochemical measurement.

bles (assigned as Au/SiO_2/CNTs) were re-dispersed in 10 mL water until use.

Next, Au/SiO_2/CNTs were used for the label of HRP-*anti*-CEA molecules. Briefly, 1.5 mL of the as-prepared Au/SiO_2/CNT solution above was initially diluted into 8.5 mL of 50 mM pH 9.0 Tris–HCl solutions, and then 500 μL HRP-*anti*-CEA ($C_{[anti\text{-}CEA]}$: 0.5 mg mL^{-1}) was thrown into the mixture and gently stirred for 12 h at 150 rpm at 4 °C. The formed bionanocables (i.e. HRP-*anti*-CEA-Au/SiO_2/CNTs) were achieved by centrifugation at 8000 rpm for 10 min at 4 °C, and dissolved in 10 mL pH 7.4 PBS containing 0.2 wt% BSA. For comparison, pure CNTs, pure Aus, and SiO_2/CNTs were also employed for the label of HRP-*anti*-CEA, i.e. HRP-*anti*-CEA-CNT, HRP-*anti*-CEA-Au and HRP-*anti*-CEA-SiO_2/CNT. The labeled methods are described in our previous papers [22,39].

2.4. Preparation of electrochemical immunosensor

Before modification, glassy carbon electrode (GCE, 2 mm in diameter) was polished with 0.3 μm and 0.05 μm alumina, followed by successive sonication in bi-distilled water and ethanol for 5 min and dried in air.

Next, the electrochemical immunosensor was prepared as the following steps: (i) 5 μL of Nafion ethanol solution (0.5%, v/v) was initially cast on the GCE, and then removed to parch with an infrared light for 5 min; (ii) the Nafion/GCE was immersed into 2.0 mM thionine acetate salt solution and 16-nm gold colloids ($C_{[Au]}$ = 24 mM), and incubated for 30 min and 360 min at RT, respectively; (iii) 20 μL *anti*-CEA antibody ($C_{[anti\text{-}CEA]}$: 0.5 mg mL^{-1}) was dropped on the surface of Au/thinone/Nafion/GCE, and incubated for 6 h at 4 °C; and (iv) the as-prepared immunosensor (assigned as *anti*-CEA/Au/TH/NF/GCE) was incubated in 0.25 wt% BSA for 60 min at 37 °C to eliminate non-specific binding effect and block the remaining active groups. The assembled process of the immunosensor is represented in Scheme 1.

2.5. Electrochemical measurement

Electrochemical measurements were carried out using a conventional three-electrode system with a modified GCE as working electrode, a platinum foil as auxiliary electrode, and a saturated calomel electrode (SCE) as reference electrode. The assay mainly consisted of the following steps: (i) *reaction with the analyte*: 10 μL of CEA standards or samples was dropped onto the surface of *anti*-CEA-modified electrode, and incubated for 12 min at RT to form the antigen–antibody complex; (ii) *conjugation with secondary antibodies*: 20 μL of HRP-*anti*-CEA-Au/SiO_2/CNT solution was thrown onto the modified electrode after slightly washing with pH 7.4 PBS, and incubated for another 12 min at RT to construct a sandwich immunocomplex; and (iii) *measurement*: the formed sandwich immunocomplex was monitored in 3 mL pH 5.5 ABS containing 5 mM H_2O_2 by using differential pulse voltammetry (DPV) from 500 to 100 mV (*vs.* SCE) with a pulse amplitude of 50 mV and a pulse width of 50 ms. The assay principle of the electrochemical immunosensor is schematically illustrated in Scheme 1.

After each immunoassay, the immunosensor was regenerated by immersing it into 0.1 M glycine-HCl (pH 2.0) for 5 min and washed with pH 7.4 PBS, and then carried out the following run cycle. The responses in all experiments were referred to the average responses of immunoreaction with corresponding standard deviations of triplicate measurements, unless otherwise indicated.

3. Results and discussion

3.1. Characteristics of HRP-anti-CEA/Au/SiO_2/CNT bionanocables

In the present work, the HRP-*anti*-CEA/Au/SiO_2/CNT bionanocables were synthesized using the sol–gel method and self-assembly technique. To prepare CNT-based symbiotic coaxial nanocables, the long carbon nanotubes were initially be shortened by using the H_2SO_4 and HNO_3 mixture. During this process, numerous carboxylate groups were generated on the CNT surface. PVP, a water-soluble polymer with positive charges, has excellent wetting properties and readily forms films in solution, which makes it as a coating or an additive to coatings [40]. So, the negatively charged silica nanoparticles could be formed and grown on the surface of PVP-modified CNTs during the synthesis process. At this condition, colloidal gold could readily assemble on the surface of amino-functionalized silica particles [41]. The nanogold-coated carbon nanotube nanoca-

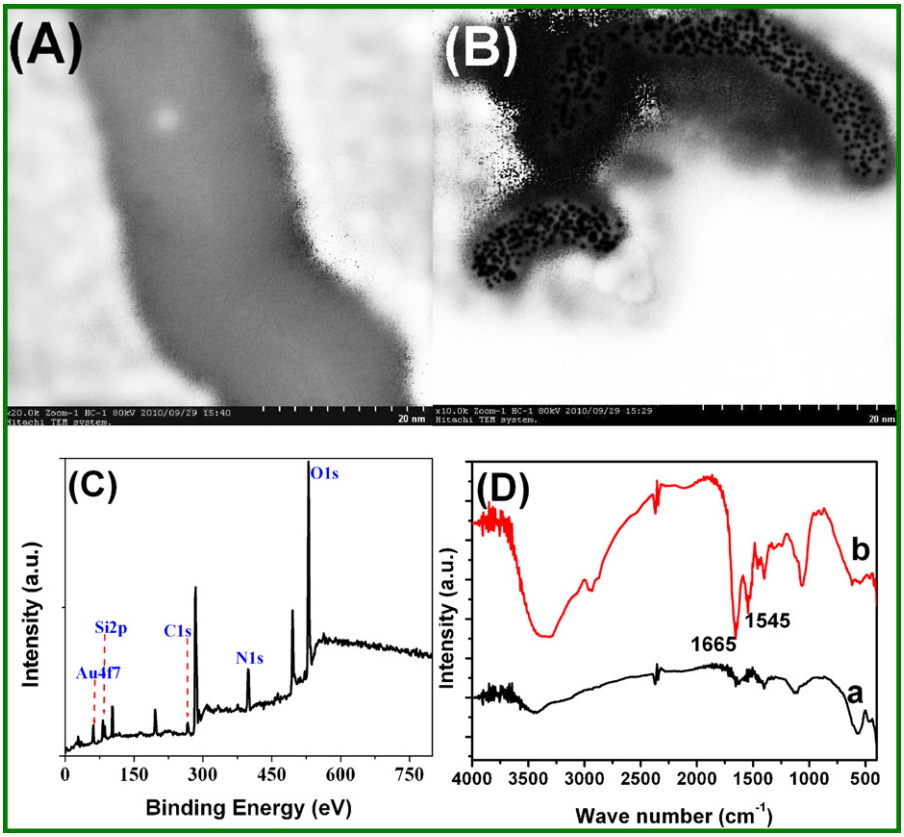

Fig. 1. TEM images of (A) SiO_2/CNT and (B) Au/SiO_2/CNT. (C) XPS spectra of the as-prepared Au/SiO_2/CNT symbiotic coaxial bionanocables. (D) FT-IR spectra of (a) Au/SiO_2/CNTs and (b) HRP-*anti*-CEA-Au/SiO_2/CNTs.

bles could provide a large room for the immobilization of HRP-*anti*-CEA.

To demonstrate the successful synthesis of HRP-*anti*-CEA/Au/SiO_2/CNT nanocables, various methods and techniques were employed including TEM, XPS and FT-IR. Fig. 1A displays the typical TEM image of the shortened carboxylated CNTs modified with silica nanoparticles, and a homogenous surface with the mean size of 8–15 nm was observed. Compared with the size of pure CNTs (5–10 nm provided by manufacturer), the size was increased 3–5 nm after the formation of SiO_2/CNTs. So, the coated silica nanolayer on the CNTs is very thin. Moreover, the thin silica nanolayer could be utilized as an affinity support for gold nanoparticles, as indicated in Fig. 1B. To further confirm the existence of Au and SiO_2 on the CNTs, XPS experiment was carried out for the surface analysis of the Au/SiO_2/CNT sample (Fig. 1C). As seen from Fig. 1C, an obvious Au4f7 signal corresponding to the binding energy of metallic Au was acquired. Meanwhile, Si2p and O1s signal characteristic of silica, a N1s signal characteristic of $-NH_2$, and a C1s signal characteristic of CNTs were also obtained. On the basis of TEM and XPS results, we might make a conclusion that carbon nanotube-based coaxial nanocables could be formed through the developed method.

Could the synthesized nanocables conjugate the biomolecules? The FT-IR spectra of the Au/SiO_2/CNTs before and after modification with HRP-*anti*-CEA were studied (Fig. 1D). As is well known, the shapes of the infrared absorption bands of amide I groups at 1610–1690 cm^{-1} corresponding to the C=O stretching vibration of peptide linkages and amide II groups around 1500–1600 cm^{-1}

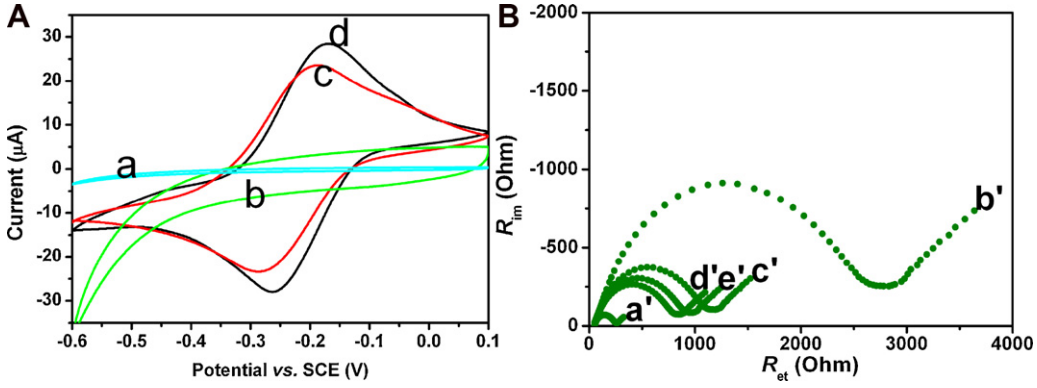

Fig. 2. (A) Cyclic voltammograms of (a) anti-CEA-Au/NF/GCE, (b) anti-CEA/Au/TH/GCE, (c) anti-CEA-TH/NF/GCE, and (d) anti-CEA/Au/TH/NF/GCE in pH 5.5 ABS at 50 mV s^{-1}; (B) EIS spectra of (a′) GCE, (b′) NF/GCE, (c′) TH/NF/GCE, (d′) Au/TH/NF/GCE, and (e′) anti-CEA/Au/TH/NF/GCE in 5 mM $Fe(CN)_6^{3-/4-}$ solution containing 0.1 M KCl.

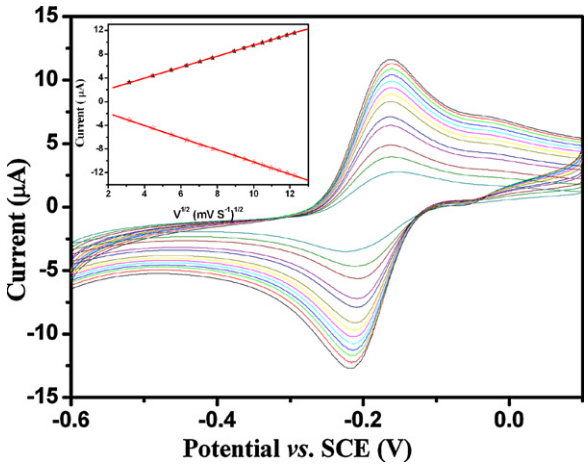

Fig. 3. Cyclic voltammograms of anti-CEA/Au/TH/NF/GCE in pH 5.5 ABS at 10, 20, 40, 50,60, 80, 90, 100, 110, 120, 130, 140, and 150 mV s^{-1} (from inner to outer). Inset: plots of peak current *vs.* $v^{1/2}$.

from a combination of N–H bending and C–N stretching can provide detailed information on the secondary structure of proteins [42]. As indicated from curve *b* of Fig. 1D, two absorption bands for amide I and amide II at HRP-*anti*-CEA/Au/SiO_2/CNTs were obtained at 1645 and 1545 cm^{-1}, respectively. This result indicated that HRP-*anti*-CEA could be conjugated on the nanocable surface through the interaction between gold colloids and proteins.

3.2. Electrochemical behaviors of variously modified electrodes

The formation of a biocomposite membrane on the modified electrode usually combines two or more phases of various natures. The complex film is not only used for immobilization of biomolecules, but also acts as a transducer. So, the binding materials are crucial for construction of the sensor. Fig. 2A represents the cyclic voltammograms of differently modified electrodes in pH 5.5 ABS at 50 mV s^{-1}. Almost no cyclic voltametric peaks were observed at both *anti*-CEA/Au/NF/GCE and *anti*-CEA/Au/TH/GCE in the working potential range in 0.1 M pH 5.5 ABS (curves *a* and *b* in Fig. 2A). A couple of stable and well-defined redox peak was obtained at *anti*-CEA/TH/NF/GCE (curve *c* in Fig. 2A) and *anti*-CEA/Au/TH/NF/GCE (curve *d* in Fig. 2A). These results indicated that the absence of thionine in the membrane could not result in the formation of redox peak compared with curves *a* and *d* in Fig. 2A. Meanwhile, curve *b* in Fig. 2A also further demonstrated that thionine as a mediator was immobilized on the electrode *via* the strong interaction between the negatively charged Nafion and the positively charged thionine. Significantly, use of gold nanoparticles was greatly improved the electrochemical properties of the modified electrode as indicated from curve *d* in Fig. 2A. Thus, the modified electrode with the help of Aus, NF and thionine could exhibit the good electrochemical behaviors.

To further verify the conclusion mentioned above and the electrochemical behaviors of the electrode during the modification, the electrochemical impedance spectroscopy (EIS) of variously modified electrodes were monitored in 5 mM $Fe(CN)_6^{3-/4-}$ solution containing 0.1 M KCl (Fig. 2B). The high frequency region of the impedance plot shows a semicircle related to the redox probe

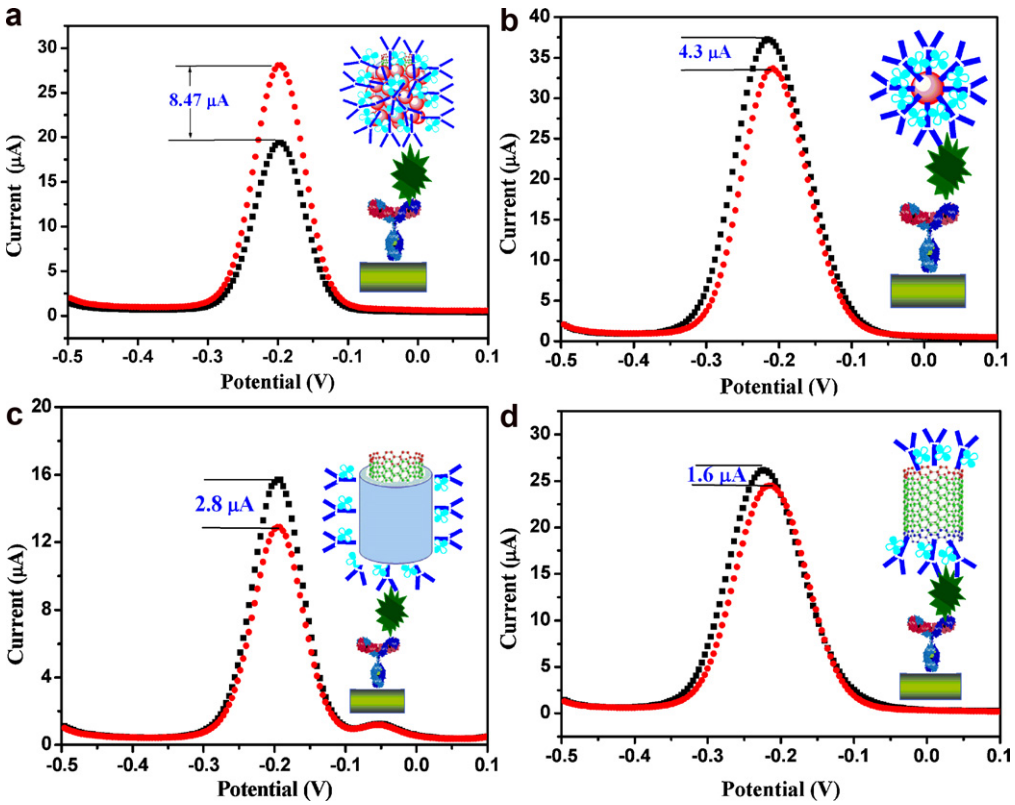

Fig. 4. DPV responses of (a) HRP-*anti*-CEA-Au/SiO_2/CNT, (b) HRP-anti-CEA-Au, (c) HRP-anti-CEA-SiO_2/CNT, and (d) HRP-*anti*-CEA-CNT toward 5 ng mL^{-1} CEA in pH 5.5 ABS without and with 5 mM H_2O_2.

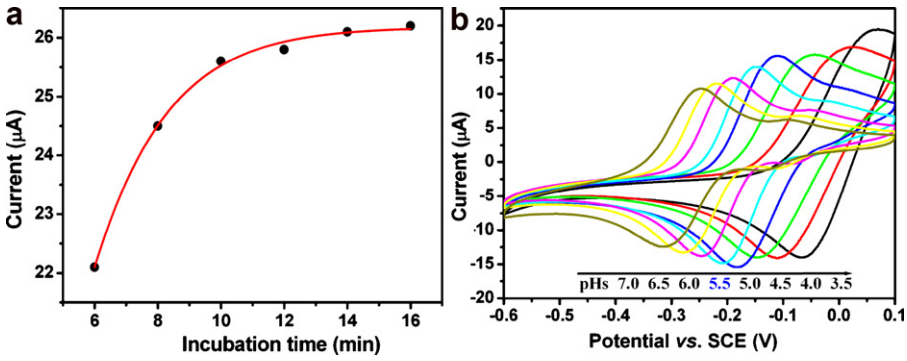

Fig. 5. The effect of (a) incubation time and (b) pH of ABS on the DPV peak currents of the electrochemical immunosensor (5 ng mL^{-1} CEA as an example).

$Fe(CN)_6^{3-/4-}$, followed by a Warburg line in the low frequency region which corresponds to the diffusion step of the overall process [43]. The bare GCE exhibited a low resistance (curve *a′* in Fig. 2B, R_{et} = 236 Ω). When Nafion was modified on the GCE surface, a high resistance was obtained (curve *b′* in Fig. 2B, R_{et} = 2723 Ω). After thionine was assembled on the surface of NF/GCE, however, the resistance was decreased (curve *c′* in Fig. 2B, R_{et} = 1196 Ω). The reason might be the fact that thionine as a mediator could facilitate the electron transfer, and the positively charged thionine could attract the negatively charged $Fe(CN)_6^{3-/4-}$. In contrast, the resistance was decreased again at the Au/NF/GCE (curve *d′* in Fig. 2B, R_{et} = 879 Ω), which was mainly attributed to the high conductivity of gold nanoparticles. *Anti*-CEA antibody as a biomacromolecule with weak electroactivity, its assembly resulted in the resistance decrease (curve *e′* in Fig. 2B, R_{et} = 987 Ω). So, the EIS results were in accordance with those of cyclic voltammetry.

Fig. 3 records the cyclic voltammograms of *anti*-CEA/Au/TH/NF/GCE at different scan rates. Both the anodic and cathodic peak currents increase with the square root of scan rate ($v^{1/2}$) in the range of 10–150 mV s^{-1}, as shown in the inset of Fig. 3, suggesting a diffusion-limited redox process.

3.3. Comparison of detection antibodies with various labels

In this contribution, the assay of analyte is based on a sandwich-type immunoassay format using HRP-*anti*-CEA-Au/SiO_2/CNTs as tracers and H_2O_2 as enzyme substrates. So, the label of detection/secondary antibody is crucial. To clarify the merits of the Au/SiO_2/CNT-based bionanocables, four detection antibodies with various labels including HRP-*anti*-CEA-CNT, HRP-*anti*-CEA-SiO_2/CNT, HRP-*anti*-CEA-Au and HRP-*anti*-CEA-Au/SiO_2/CNT were used for detection of 5 ng mL^{-1} CEA as an example using the *anti*-CEA/Au/TH/NF/GCE. The judgement is based on the shift in DPV peak currents of the sandwiched immunocomplex-modified electrode in pH 5.5 ABS at the absence and presence of 5 mM H_2O_2 (Fig. 4). As seen from Fig. 4, we might find that the electrochemical immunosensor exhibited larger current shifts using nanogold-modified probes as detection antibodies (curves *a* and *b*) than those without nanogold particles (curves *c* and *d*). The reason might be attributed to the fact that HRP-*anti*-CEA molecules were covalently conjugated onto the CNTs and SiO_2/CNTs by using glutaraldehyde as linker, while those were immobilized on the nanogold surface through the strong interaction between the protein and nanogold particles. So, use of gold nanoparticles could provide an advan-

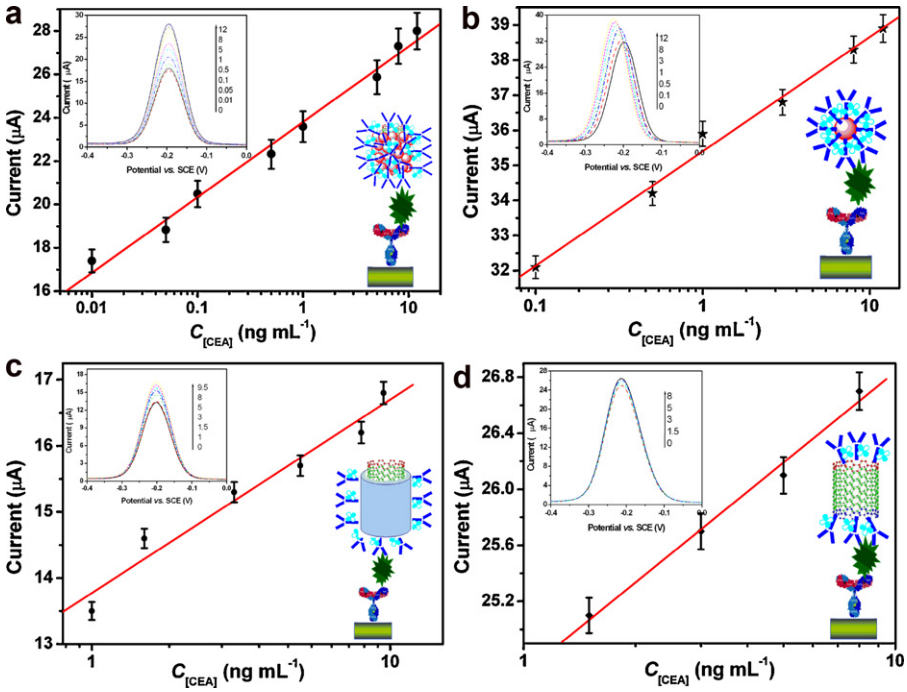

Fig. 6. Calibration curves of the electrochemical immunosensor toward CEA standards in pH 5.5 ABS containing 5 mM H_2O_2 by using (a) HRP-*anti*-CEA-Au/SiO_2/CNT, (b) HRP-anti-CEA-Au, (c) HRP-anti-CEA-SiO_2/CNT, and (d) HRP-*anti*-CEA-CNT as detection antibodies, respectively. Insets: DPV curves corresponding to linear plots.

Table 1
The interference degree of variability between lineage-different biomarkers.

$C_{[CEA]}$ (ng mL^{-1})	$C_{[AFP]}$ (ng mL^{-1})/DPV peak current (μA)[a]				Mean ± SD (μA)	RSD (%)
	0	0.5	5	10		
0	16.3	16.6	16.4	16.7	16.5 ± 0.16	1.0
0.5	22.3	22.8	23.2	23.7	23.0 ± 0.52	2.3
5	25.9	25.7	26.4	26.1	26.1 ± 0.29	1.1
10	27.5	26.7	28.2	27.9	27.6 ± 0.57	2.1

[a] The average value of three successful assays.

Table 2
The recoveries assayed by using the electrochemical immunosensor *via* spiking CEA standards into 0.01 M pH 7.4 PBS.

Sample no.	Spiking value (ng/mL)	Assayed value (mean ± SD, ng/mL)[a]	Recovery (%)
1	0.5	0.52 ± 0.04	104
2	2.0	1.98 ± 0.12	99
3	5.0	5.31 ± 0.45	106.2
4	8.0	8.87 ± 0.78	110.9
5	11.0	10.43 ± 0.97	94.8

[a] The average of three successful assays.

tage for the label of HRP-*anti*-CEA due to high surface-to-volume ratio and good biocompatibility of gold colloids. More significantly, the electrochemical responses could be improved by using HRP-*anti*-CEA-Au/SiO_2/CNTs (Fig. 4a) in comparison with that of using HRP-*anti*-CEA-Au (Fig. 4b). The reason might be suspected that carbon nanotube could provide more room for the attachment of gold nanoparticles, which indirectly increased the binding amount of HRP-*anti*-CEA. When one antibody on the Au/SiO_2/CNT reacted with antigen on the electrode, other HRP-*anti*-CEA molecules were loaded up and participated in the catalytic reaction.

3.4. Optimization of experimental conditions

To acquire an optimal analytical performance of the as-prepared immunosensor, some experimental parameters including the incubation time and incubation temperature for the antigen–antibody reaction and pH of assay solution. Of course, the optimum incubation temperature of antigen–antibody interaction should be close to the normal temperature of human body (37 °C). Considering the practical feasibility in real life, however, room temperature (RT) should be preferable. Therefore, all experiments in this study were carried out at RT.

The incubation time is a bottleneck to the improvement of immunoassay efficiency, which is usually controlled by mass transport of immunoreagents and kinetics of immunoreaction. Due to large surface-to-volume ratio of Au/SiO_2/CNTs, it was beneficial to accelerating the immunoreaction for the formation of sandwich-type immunocomplex. Fig. 5a displays the electrochemical responses of the immunosensor in pH 5.5 ABS containing 5 mM H_2O_2 after incubated with 5 ng mL^{-1} (as an example) for various times. The DPV peak currents increased with the increasing incubation time, and trended to level off after 12 min, and longer incubation time could not improve the response. Thus, 12 min was used for the antigen–antibody reaction.

Fig. 5b shows the cyclic voltammograms of the immunosensor in 0.1 M ABS with various pH values at 50 mV s^{-1} after incubated with 5 ng mL^{-1} CEA and excessive bionanocables. As indicated from Fig. 5b, the peak currents decreased with increase of pH value from 3.5 to 7.0, while the potential separation of anodic peak and cathodic peak increased. At pH 5.5 ABS, the electrochemical immunosensor exhibited a quasi-reversible redox process (i.e. $\Delta E_p \approx 60$ mV and $i_{pc}/i_{pa} \approx 1$). Meanwhile, we also considered that higher or lower pH might affect the bioactivity of the immobilized proteins. So, pH 5.5 ABS was selected for the detection of CEA.

3.5. Electrochemical response of the immunosensor toward CEA standards

Under optimal conditions, the sensitivity and dose–response curve of the proposed immunosensor were evaluated toward various concentrations of CEA standards by using the as-synthesized bionanocables as detection antibodies with a DPV measurement in pH 5.5 ABS containing 5 mM H_2O_2. As seen from Fig. 6a, the cathodic peak currents of the immunosensor increased with the increment of CEA concentrations, and exhibited a linear relationship between the DPV peak currents and the logarithm of CEA concentrations from 0.01 to 12 ng mL^{-1}. The linear regression equation was adjusted to I (μA) = 23.8 + 1.51 × ln $C_{[CEA]}$ (ng mL^{-1}, R^2 = 989) with a detection limit (LOD) of 5 pg mL^{-1} CEA at a signal to noise ratio of 3σ (where σ is the standard deviation of the blank, n = 12). Since the normal range of CEA in human serum is less than 10 ng mL^{-1}, the sensitivity of the electrochemical immunosensor was enough to practical application. When the CEA concentration was higher than 12 ng mL^{-1}, an appropriate dilution was preferable in the pre-incubation step. For comparison, other labeling probes including HRP-*anti*-CEA-SiO_2/CNT, HRP-*anti*-CEA-CNT and HRP-*anti*-CEA-Au were also employed for detection of CEA using the same mode at the anti-CEA/Au/Th/NF/GCE, respectively. The

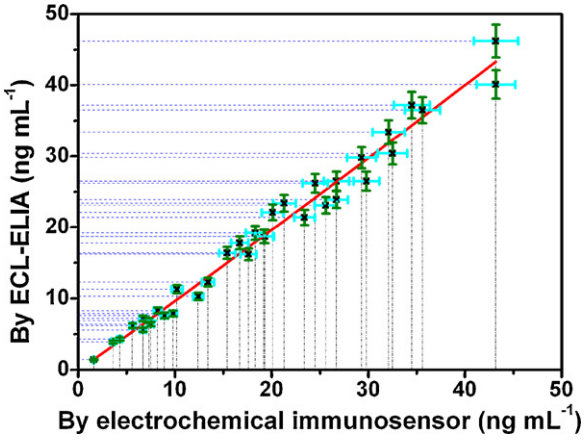

Fig. 7. Comparison of assay results for clinical serum specimens by using the electrochemical immunosensor and the ECL-ELIA reference method.

Table 3
Comparison of analytical properties of the developed immunosensor with those of other CEA electrochemical immunosensors and immunoassays.

Modified electrode	Linear range (ng mL^{-1})	LOD (ng mL^{-1})	Signal antibody	Ref.
Au/Fe_3O_4	0.1–220	0.01	Label-free	[44]
Au/TiO_2	0.2–160	0.06	Label-free	[45]
AgNP/DNA/Nafion	0.03–32	0.01	Label-free	[46]
Au	0.05–50	0.048	Au labels	[47]
Au/proussian blue	0.05–350	0.01	Au/graphene labels	[48]
Au/Fe_3O_4	0.005–50	0.001	Label-free	[49]
Glassy carbon disk	0.01–80	0.0033	Quantum dot barcodes	[50]
Au/prossian blue	0.002–2.0	0.0014	Au/Prussian blue/CNTs	[51]
CNT	0.005–500	0.001	Liposomes	[52]
Carbon nanparticles	0.032–10	0.032	Quantum dots	[53]
Au/TH/NF	0.01–12	0.005	Au/SiO_2/CNT	This work

linear range, regression equation and detection limit (LOD) are listed as follows:

(i) Using HRP-*anti*-CEA-Au as detection antibodies (Fig. 6b): 0.1–12 ng mL^{-1}, I (μA) = 35.4 + 1.37 × ln $C_{[CEA]}$ (R^2 = 0.985) and 0.05 ng mL^{-1} CEA.
(ii) Using HRP-*anti*-CEA-SiO_2/CNT as detection antibodies (Fig. 6c): 1.0–8.0 ng mL^{-1}, I (μA) = 13.8 + 1.27 × ln $C_{[CEA]}$ (R^2 = 0.96) and 0.1 ng mL^{-1} CEA.
(iii) Using HRP-*anti*-CEA-CNT as detection antibodies (Fig. 6d): 1.5–9.5 ng mL^{-1}, I (μA) = 24.6 + 1.04 × ln $C_{[CEA]}$ (R^2 = 0.973) and 0.5 ng mL^{-1} CEA.

Thus, the electrochemical immunoassay using HRP-*anti*-CEA-Au/SiO_2/CNT could exhibit wider linear range and lower LOD.

3.6. Precision, selectivity, stability of the electrochemical immunosensors

The precision of the electrochemical immunosensor was monitored by calculating the intra- and inter-batch variation coefficients (CVs). As indicated from experimental results, the CVs of the assays using HRP-*anti*-CEA-Au/SiO_2/CNT from the same batch were 7.8, 6.9, and 9.3% at 1.0, 5,0 and 10 ng mL^{-1} CEA levels, respectively, while the CVs of the assays using the bionanocables from different batches were 9.1, 6.2, and 8.8% at the above-mentioned analyte concentrations. The sensor-to-sensor reproducibility was investigated using the same-batch bionanocables for the detection of 10 ng mL^{-1} CEA (as an example). The CV value was 9.1% for 5 immunosensors. The electrochemical immunoassay exhibited satisfactory stability. In fact, as much as 90% of the initial DPV response was preserved after storage of the immunosensor and HRP-*anti*-CEA-Au/SiO_2/CNT at 4 °C for 21 days.

To evaluate the specificity of the electrochemical immunosensor, we challenged the system with other biomarkers, e.g. cancer antigen 125 (CA 125), prostate-specific antigen (PSA), alpha-fetoprotein (AFP) and BSA. The specificity was studied by using an incubation solution containing the known CEA standards and interfering agents with various concentrations. Table 1 represents the results by using AFP as an example. As seen from experimental results, no obvious difference of DPV peak current was observed toward various concentrations of interfering agents in comparison with the results obtained in the presence of only CEA at 0.5, 5 and 10 ng mL^{-1}. Moreover, the concentration increase of the interfering agents did not lead to a significant current shift to some extent. Furthermore, after the immunosensor was incubated in 5 ng mL^{-1} followed by rinsing with stripping buffer of pH 2.0 glycine-HCl to remove the CEA from the immunocomplex, the obtained current signal at 7th time could restore the ~90% of the initial value. So, the immunosensor had a good selectivity to CEA as well as an acceptable regeneration.

3.7. Analysis of human serum samples and interlaboratory validation

To investigate the feasibility of the developed method for the analysis of real sample, two methods were performed. The first method is to spike the CEA standards into pH 7.4 PBS, and the content of CEA was assayed by using the electrochemical immunosensor. As seen from Table 2, the recovery was from 94.8% to 110.9%. The reason for higher recoveries might be attributed to the fact that the antigen–antibody linkage was not completely broken during the regeneration, and thus the binding antigens on the electrode might be indirectly increased the conjugated amount of HRP-*anti*-CEA-Au/SiO_2/CNT. In this regard, the recovery of the immunosensor was acceptable.

Further, 35 human serum specimens were evaluated using the electrochemical immunosensor, and the obtained results were compared with those by commercially available electrochemiluminescent enzyme-linked immunoassay (ECL-ELIA) as a reference method (Fig. 7) (note: the sample was diluted by using 0.01 M pH 7.4 PBS when the concentration of CEA was higher than 12 ng mL^{-1}). The experimental results obtained by two methods were fitted to a regression equation: $y = (1.007 \pm 0.121)x - (0.353 \pm 2.13)$ (R^2 = 0.980) where x stands for the CEA concentrations estimated with the immunoassay and y stands for those of the electrochemiluminescent. No significance differences were encountered between the optimum values of intercept and slope and experimental data, thereby revealing a good agreement between both analytical methods.

3.8. Comparison with other CEA electrochemical immunosensors

To further elucidate the advantages of the developed immunosensor, the analytical properties of the electrochemical immunosensor were compared with those of other CEA electrochemical immunosensors. These issues mainly consisted of modified electrode, linear range, LOD and detection antibody. The results are summarized in Table 3. Although the linear range was relatively narrow in comparison with those of other nanoscale-labeled probes, the LOD was comparably low. However, we might predict that the linear range can be tuned further by more professionally fabricated process for the synthesis of the HRP-*anti*-CEA-Au/SiO_2/CNTs, e.g. using the homogeneous CNTs with the same length, the level of HRP-*anti*-CEA on the nanocables, and alternative silica thinness, especially by controlling the immobilizing amount of gold nanoparticles on each CNT surface.

4. Conclusion

This work describes a facile and sensitive electrochemical immunosensor for determination of CEA by using Au/SiO_2/CNT-based symbiotic coaxial nanocables as labels. Self-assembly

technique and sol–gel method were utilized for the synthesis of Au/SiO_2/CNT nanocables, which were characterized by using FT-IR, TEM and XPS. Experimental results indicated that the analytical properties of the electrochemical immunosensor could be improved with the aid of Au and CNTs. Compared with our previous reports on the magnetic nanoparticles/nanogold-based bionanolabels [20–25], the nanocables-based bionanolabels could display low LOD and high sensitivity. So, the electrochemical immunosensor could be applied for detection of CEA with low concentration. Highlight of this work is to construct a new carbon nanotube-based bionanolabel for the amplification of assay signal. This research could open new avenues in the application of CNT-based nanocables for clinical immunoassays, and provide a convenient platform to modify for clinical testing and drug screening. Further work is underway in our labs.

Acknowledgements

This work was financially supported by the National Natural Science Foundation of China (21075019, 20877019, 20735002), the National "973" Basic Research Program of China (2010CB732403), the Key Natural Sciences Foundation of Fujian Province, China (D0520001), the Key Program of Science and Technology Department of Fujian Province, China (2007Y0026), and NTU-MOE Academic Research Funds (RG65/08).

References

[1] P. Yanez-Sedeno, J. Pingarron, J. Riu, F. Rius, TrAC-Trend. Anal. Chem. 29 (2010) 939.
[2] C. Jacobs, M. Peairs, B. Venton, Anal. Chim. Acta 662 (2010) 105.
[3] H. Chen, C. Jiang, C. Yu, S. Zhang, B. Liu, J. Kong, Biosens. Bioelectron. 24 (2009) 3399.
[4] http://www.tc-cancer.com/tumormarkers.html.
[5] http://www.herbalzym.com/2010/05.
[6] S. Mascini, S. Tombelli, Biomarkers 13 (2008) 637.
[7] C. Lin, J. Wang, H. Wu, G. Lee, JALA-J. Assos. Lab. Autom. 15 (2010) 253.
[8] Y. Yuan, R. Yuan, Y. Chai, Y. Zhuo, L. Mao, S. Yuan, J. Electroanal. Chem. 643 (2010) 15.
[9] Y. Wang, Z. Zhang, V. Jain, J. Yi, S. Mueller, J. Sokolov, Z. Liu, M. Rafilovich, Sens. Actuators B 146 (2010) 381.
[10] U. Lad, S. Khokhar, G. Kale, Anal. Chem. 80 (2008) 7910.
[11] M. Pohanka, P. Skladal, J. Appl. Biomed. 6 (2009) 57.
[12] D. Knopp, D. Tang, R. Niessner, Anal. Chim. Acta 647 (2009) 14.
[13] G. Liu, Y. Lin, Talanta 74 (2007) 308.
[14] Q. Wei, X. Xin, B. Du, Y. Han, Y. Zhao, Y. Cai, M. Yang, H. Li, Biosens. Bioelectron. 26 (2010) 723.
[15] M. Yang, A. Javadi, H. Li, S. Gong, Biosens. Bioelectron. 26 (2010) 560.
[16] J. Zhang, B. Ting, M. Khan, M. Pearce, Y. Yang, Z. Gao, J. Ying, Biosens. Bioelectron. 26 (2010) 418.
[17] Y. Yuan, R. Yuan, Y. Chai, Y. Zhuo, L. Bai, Y. Liao, Anal. Biochem. 405 (2010) 121.
[18] Q. Wei, Z. Xiang, J. He, G. Wang, H. Li, Z. Qian, M. Yang, Biosens. Bioelectron. 26 (2010) 627.
[19] Z. Song, R. Yuan, Y. Chai, Y. Zhuo, W. Jiang, H. Su, X. Che, J. Li, Chem. Commun. 46 (2010) 6750.
[20] D. Tang, R. Yuan, Y. Chai, Anal. Chem. 80 (2008) 1582.
[21] D. Tang, J. Ren, Anal. Chem. 80 (2008) 8064.
[22] D. Tang, J. Tang, B. Su, G. Chen, J. Agric. Food Chem. 58 (2010) 10824.
[23] D. Tang, J. Tang, B. Su, G. Chen, Biosens. Bioelectron. 26 (2010), doi:10.1016/j.bios.2010.09.012.
[24] J. Tang, B. Su, D. Tang, G. Chen, Biosens. Bioelectron. 25 (2010) 2657.
[25] D. Tang, B. Su, J. Tang, J. Ren, G. Chen, Anal. Chem. 82 (2010) 1527.
[26] X. Li, Y. Liu, L. Fu, L. Cao, D. Wei, Y. Wang, G. Yu, J. Phys. Chem. C 111 (2007) 509.
[27] I. Willner, B. Willner, Nano Lett. 10 (2010) 3805.
[28] S. Guo, L. Huang, E. Wang, New. J. Chem. 31 (2007) 575.
[29] C. Liu, H. Zhang, Nanoscale 2 (2010) 1901.
[30] J. Jung, M. Park, S. Shinkai, Chem. Soc. Rev. 39 (2010) 4286.
[31] T. Lin, H. Shen, Nanotechnology 21 (2010) (art. no. 365604).
[32] M. Peng, J. Qi, Z. Zhou, Z. Liao, Z. Zhu, H. Guo, Langmuir 26 (2010) 13062.
[33] M. Zhang, Y. Wu, X. Feng, X. He, L. Chen, Y. Zhang, J. Mater. Chem. 20 (2010) 5835.
[34] K. Lee, R. Wi, M. Imran, T. Park, J. Lee, S. Lee, D. Kim, ACS Nano 4 (2010) 3933.
[35] M. Pumera, T. Sasaki, B. Smid, Chem. Asian J. 4 (2009) 662.
[36] S. Song, Y. Qin, Y. He, Q. Huang, C. Fan, H. Chen, Chem. Soc. Rev. 39 (2010) 4234.
[37] S. Guo, S. Dong, E. Wang, J. Phys. Chem. 112 (2008) 2389.
[38] R. Yuan, D. Tang, Y. Chai, X. Zhong, Y. Liu, J. Dai, Langmuir 20 (2004) 7240.
[39] D. Tang, Z. Zhong, R. Niessner, D. Knopp, Analyst 134 (2009) 1554.
[40] F. Chimlenko, I. Korobova, O. Gurtovaya, T. Chmilenko, Talanta 78 (2009) 1259.
[41] W. Dungchai, W. Siangproh, W. Chaicumpa, P. Tongtawa, O. Chailapakul, Talanta 77 (2008) 727.
[42] C. Flach, P. Cai, R. Mendelsohn, Springer Series Biophys. 10 (2006) 49.
[43] N. Atta, M. El-Kady, Talanta 79 (2009) 639.
[44] H. Chen, J. Tang, B. Su, G. Chen, J. Huang, D. Tang, Anal. Chim. Acta 678 (2010) 169.
[45] Y. Zhang, R. Yuan, Y. Chai, Y. Xiang, X. Qian, H. Zhang, J. Colloid Interface Sci. 348 (2010) 108.
[46] W. Wu, P. Yi, P. He, T. Jing, K. Liao, K. Yang, H. Wang, Anal. Chim. Acta 673 (2010) 126.
[47] M. Liu, C. Jia, Q. Jin, X. Lou, S. Yao, J. Xiang, J. Zhao, Talanta 81 (2010) 1625.
[48] Z. Zhong, W. Wu, D. Wang, D. Wang, J. Shan, Y. Qing, Z. Zhang, Biosens. Bioelectron. 25 (2010) 2379.
[49] J. Li, H. Gao, Z. Chen, X. Wei, C. Yang, Anal. Chim. Acta 665 (2010) 98.
[50] Y. Xiang, Y. Zhang, Y. Chang, Y. Chai, J. Wang, R. Yuan, Anal. Chem. 82 (2010) 1138.
[51] G. Lai, F. Yan, H. Ju, Anal. Chem. 81 (2009) 9730.
[52] S. Viswanathan, C. Rani, A. Vijay Anand, J. Ho, Biosens. Bioelectron. 24 (2009) 1984.
[53] J. Ho, Y. Lin, L. Wang, K. Hwang, P. Chou, Anal. Chem. 81 (2009) 1340.